Supporting Information

Control of the film stoichiometry

$SrTiO_3$-$CoFe_2O_4$ thin films were deposited at different temperatures as a method to control Sr stoichiometry. The temperatures during the synthesis procedures provided in this manuscript are nominal values with the actual temperature in all cases being approximately 150 °C lower. The sample was characterized by x-ray diffraction. The out-of-plane and in-plane lattice parameters of both CFO and STO in the composite films were obtained through 2θ scans measured along the out-of-plane and in-plane orientations of the thin film sample as shown in Figure S1a and S1b, respectively. It can be seen that both constituents are (001) oriented and that there is no intermixing between STO and CFO phases. The lattice parameters obtained by X-ray diffraction are shown in Figure S1c and the estimated tetragonality values are shown in Figure S1d. For STO, the deposited films were fully strained for the entire range of temperatures. This ensures the out-of-plane lattice parameter - and therefore tetragonality - changes as a function of the film Sr stoichiometry. The increase in the out-of-plane lattice parameter upon decreasing the growth temperature can be understood in terms of cation mobility, as the temperature is not high enough to allow migration of cation-non-stoichiometry-related defects[1]. Sr-partial-Schottky defects are energetically favored over Ti-partial-Schottky defects[2]. To avoid such Schottky-type defects, it is necessary to deposit the films at temperatures higher than half the melting point of STO (~ 2350 K) to enhance the macroscopically homogenous film stoichiometry[3]. The growth of this material below ~ 1600 K (as is the case of the films studied in this manuscript) enhances the formation of defects, which exerts a strong influence on the sample properties[4].

In CFO, tetragonality is approximately constant with increasing growth temperatures while the in-plane and out-of-plane lattice parameters both approach the ideal cubic symmetry in the bulk (8.38 Å)[5]. There are two main reasons for the change in the lattice parameters: the epitaxy imposed to the film, and/or a change in the Fe/Co stoichiometry. The in-plane lattice parameter of CFO is different to that of the substrate, implying that STO does not impose any epitaxial strain. Therefore, the changes in the unit cell parameters take place because of a modification of the Fe:Co ratio above the nominal 2:1 value[6].

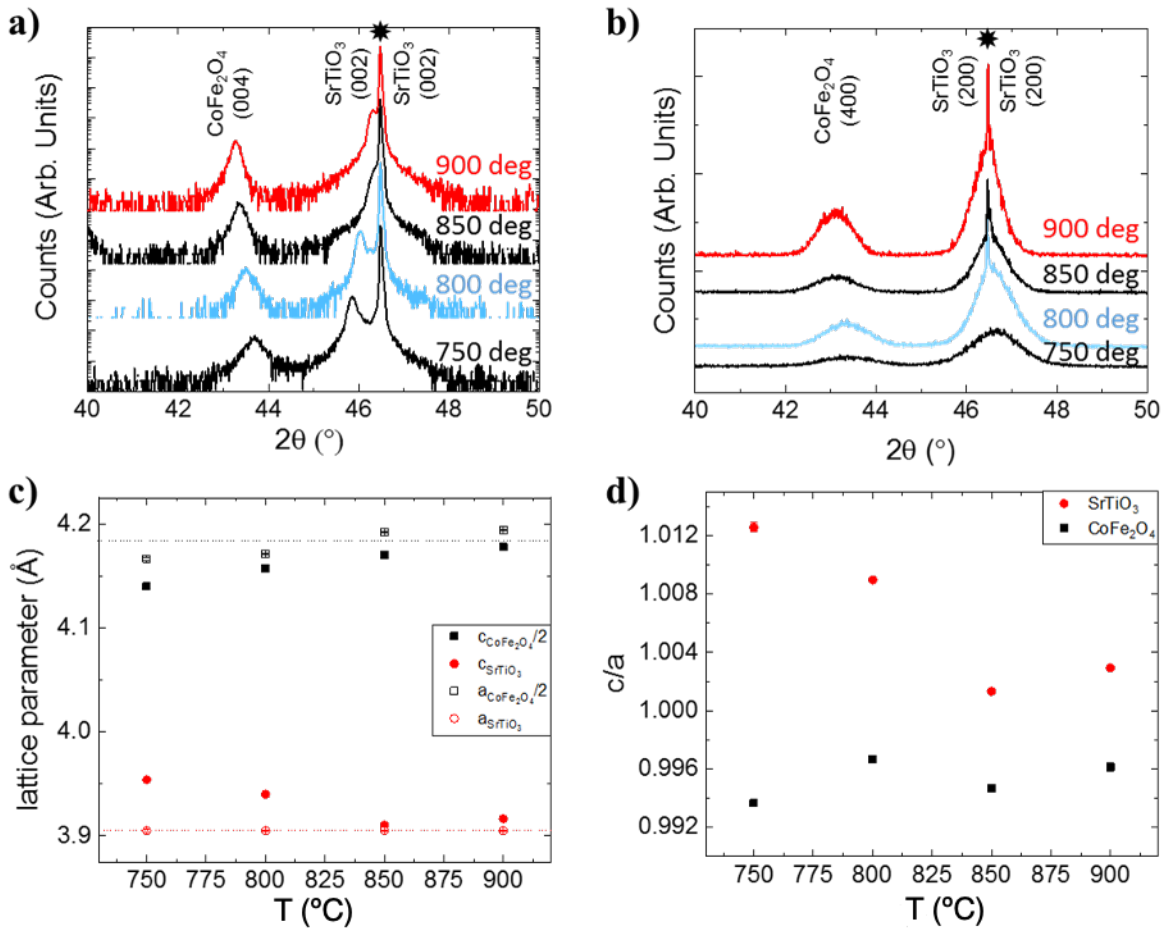

Figure S1*:* Dependence of the unit cell of $SrTiO_3$ and $CoFe_2O_4$ on the growth temperature for the self-assembled thin films. X-ray diffraction symmetric 2θ scans along the a) out-of-plane and b) in plane direction of the $SrTiO_3$ substrate. c) In plane and out-of-plane lattice parameters for both constituents. Black and red dashed lines indicate the nominal value in bulk. Note that the lattice parameter measured for $CoFe_2O_4$ is divided by a factor of two for clarity. d) Tetragonality of the $SrTiO_3$ and $CoFe_2O_4$ unit cells.

Scanning transmission electron microscope (STEM) cross section

In order to verify that nanocolumns span all the film thickness, we have extracted a lamella out of the film using a focus ion beam (FIB). Subsequently a bright field STEM image and EDX-maps (not shown here) of the lamella were acquired. Both confirmed that the columns extend through the thickness of the film. The TEM used was a probe corrected NeoARM (JEOL) operated at 200kV.

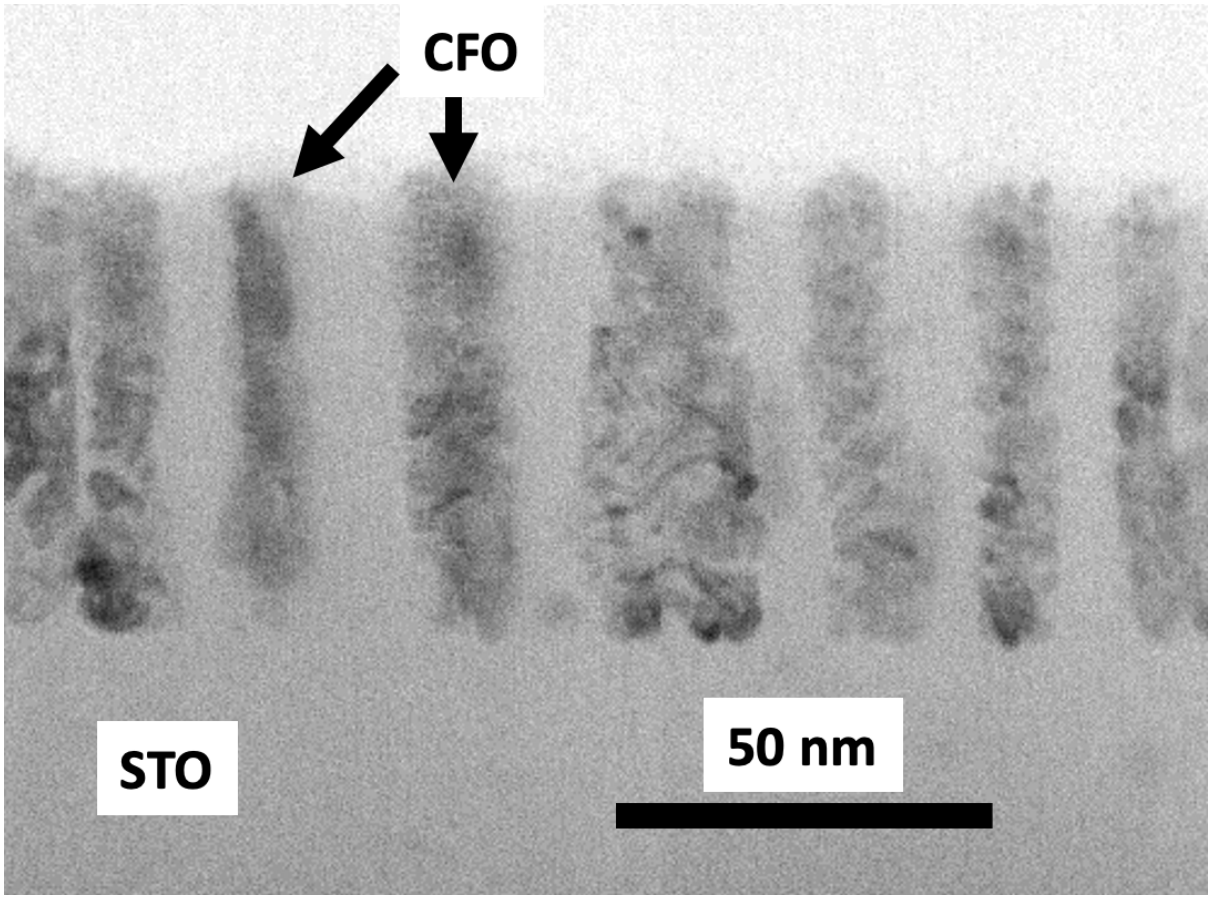

Figure S2: *Bright field STEM image. At the lower part of the image, the STO substrate is visible. The layer above the substrate is composed of CFO nanocolumns embedded in the STO matrix. The columns extend through the whole thickness of the layer and consist of small CFO crystallites. From the diffraction pattern we ascertained that the crystallites are well aligned with the STO basic lattice.*

Simulations

The experimental Ti $L_{2,3}$ XAS and XLD spectra for grazing incident geometry (see Fig. S3) were simulated using the CTM4XAS program[7]. The broadening of the absorption spectra due to the core-hole life time was modelled using a Lorentzian function of width Γ. The following values for Γ were used: 0.1 eV and 0.6 eV at the L_3 edge for t_{2g} and e_g states, respectively. 0.5 eV and 1 eV at the L_2 edge for t_{2g} and e_g states, respectively[8]. All peaks were convoluted with a Gaussian broadening of $0.15\ eV$. The charge transfer energy Δ was fixed at $3\ eV$, and the Coulomb interactions $U_{dd} = 6\ eV$ and $U_{pd} = 8\ eV$.

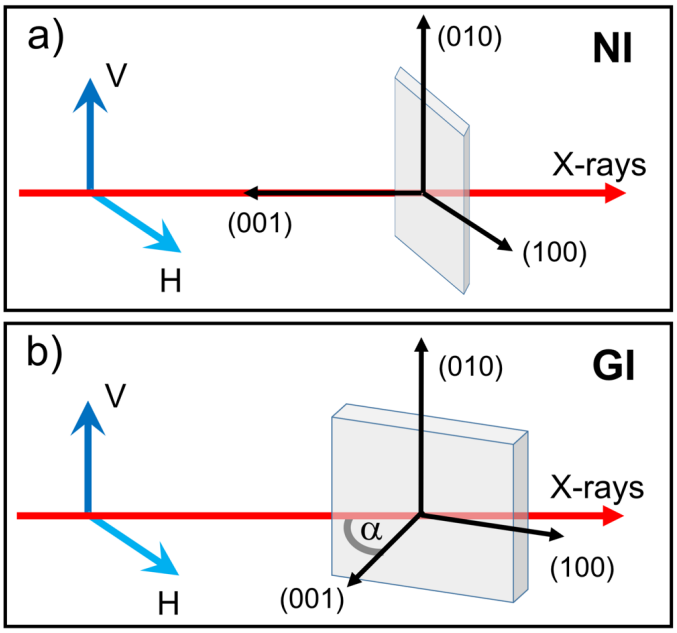

Figure S3: Experimental geometry. X-rays with horizontal (H) or vertical (V) polarization impinge on the sample. a) Normal incident (NI) geometry. The X-rays are parallel to the (001) crystallographic direction. b) Grazing incident (GI) geometry. The X-rays are at an angle of α=60º to the (001) crystallographic direction.

First the dependence of the XAS spectrum on the crystal field splitting energy ($10D_q$) between the e_g and t_{2g} orbital state is shown (Figure S4 top left). On increasing $10D_q$, the XAS t_{2g} (e_g) peaks at both the L_2 and L_3 edges are shifted toward lower (higher) energy values, in addition to a modification in the intensities of the t_{2g} and e_g peaks. If only $10D_q$ (with D_s=D_t=0) is included, the point symmetry of Ti^{4+} is octahedral, as in cubic STO. In this case the XLD is zero. The best value found for our films is $10D_q = 1.9\ eV$.

Next, the effects of a tetragonal distortion on the XAS and XLD spectra were analyzed. The dependence of the energy splitting of the orbital states under this geometry is sketched in Figure S4. Upon increasing the $|D_s|$ energy, the XAS spectrum remains almost constant and the intensity of the XLD peaks increases (Figure S4 top right). Also, all the XLD peaks remain symmetric in intensity around the zero baseline. When including the D_t term, a change in the XAS spectra occurs: the XAS e_g peaks shift towards lower energy values as well as displaying a change in the e_g/t_{2g} intensity ratio (Figure S4 bottom left). As a consequence, the spectral changes in the XLD are not symmetric around zero intensity anymore. To fit the experimental results measured in our samples, both D_s has to be decreased and D_t needs to be increased. The dependence of the XAS and XLD spectra on D_t with $D_s = -0.03\ eV$ is shown in the bottom

right part of Figure S5. The best fit to our experimental results is achieved for $D_S = -0.03\ eV$ and $D_t = 0.03\ eV$.

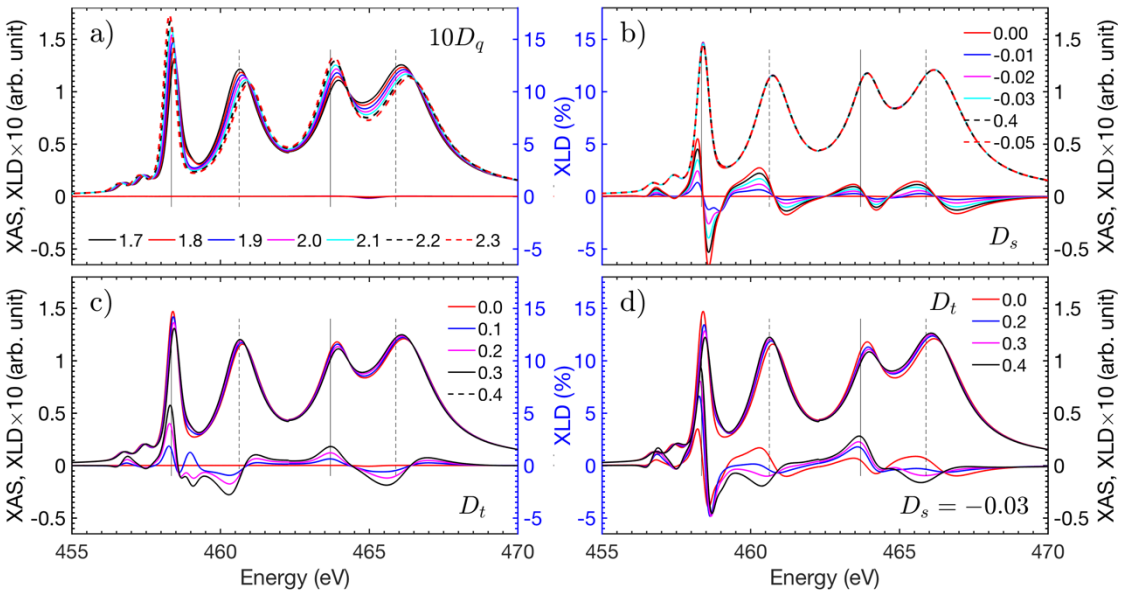

Figure S4: Simulations of the dependence of the XAS and XLD spectrum on $10D_q$ (top left), D_s (top right), D_t (bottom left), and D_t with $D_s = 0.03$ eV (bottom right). The black lines indicate the position of the maximum of the L_2 and L_3, t_{2g} and e_g peaks of the experimental data measured at room temperature.

Finally, to account for the covalency of Ti^{4+} 3*d*- with O^{2-} 2*p*-orbitals, charge transfer parameters were included in the calculations[7]. These parameters were considered for the four charge-transfer energies with tetragonal symmetry; T_{b1}, T_{a1}, T_{b2}, T_e corresponding to $d_{x^2-y^2}, d_{z^2}, d_{xy}$ and d_{xz} (d_{yz}) orbitals, respectively. Upon modifying these parameters, the XAS spectra remain constant in all cases while noticeable variations are seen in the XLD spectra (Figure S5). As an increase of covalency in one orbital is linked to a decrease of covalency in the perpendicularly oriented orbital, an increase in T_{b1} (T_{b2}) has the same influence in the XLD spectra as a decrease in $T_{a1}(T_e)$. Our simulations led to the following conclusion: as observed experimentally, it is only possible to obtain an enhancement of the XLD e_g peak without any substantial modification of the XAS spectrum only if the charge-transfer parameters are increased for orbitals along the *xy*-plane. The black lines indicate the position of the maximum of the L_2 and L_3, t_{2g} and e_g peaks of the experimental data measured at room temperature.

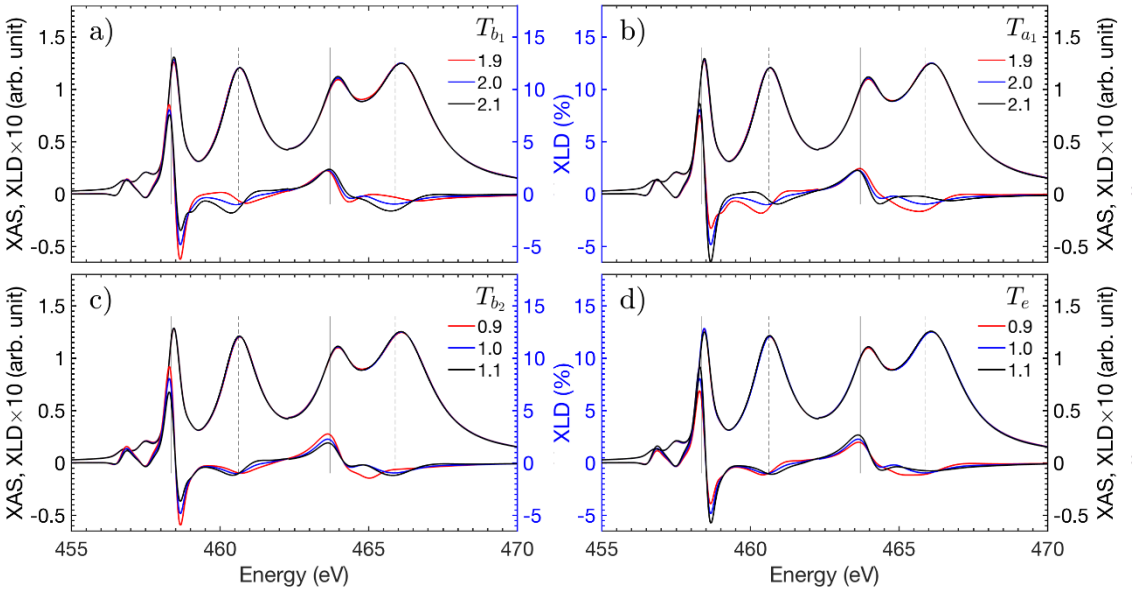

***Figure S5**:* Simulation of the dependence of the XAS and XLD spectra on the charge transfer parameters for $T_{b1}(d_{x^2-y^2})$ orbitals (top left); $T_{a1}(d_{z^2})$ orbitals (top right); $T_{b2}(d_{xy})$ orbitals (bottom left); and $T_e(d_{xz}/d_{yz})$ orbitals (bottom right). Values: Dq=1.9, Ds=-0.03, Dt=0.03, Delta =3, Upd =8, Udd=6. The black lines indicate the position of the maximum of the L_2 and L_3, t_{2g} and e_g peaks of the experimental data measured at room temperature.

References Supplementary

1. P. Ambwani, P. Xu, G. Haugstad, J. S. Jeong, R. Deng, K. A. Mkhoyan, B. Jalan and C. Leighton, *J Appl Phys*, 2016, **120**. http://dx.doi.org/10.1063/1.4960343.
2. T. Tanaka, K. Matsunaga, Y. Ikuhara and T. Yamamoto, *Phys Rev B*, 2003, **68**. http://dx.doi.org/10.1103/PhysRevB.68.205213.
3. Y. Kozuka, Y. Hikita, C. Bell and H. Y. Hwang, *Appl Phys Lett*, 2010, **97**. http://dx.doi.org/10.1063/1.3457994.
4. T. Ohnishi, K. Shibuya, T. Yamamoto and M. Lippmaa, *J Appl Phys*, 2008, **103**. http://dx.doi.org/10.1063/1.2921972.
5. D. T. Margulies, F. T. Parker, F. E. Spada, R. S. Goldman, J. Li, R. Sinclair and A. E. Berkowitz, *Phys Rev B*, 1996, **53**, 9175-9187. http://dx.doi.org/10.1103/PhysRevB.53.9175.
6. P. C. Dorsey, P. Lubitz, D. B. Chrisey and J. S. Horwitz, *J Appl Phys*, 1996, **79**, 6338-6340. http://dx.doi.org/10.1063/1.361991.
7. M. U. Delgado-Jaime, K. L. Zhang, J. Vura-Weis and F. M. F. de Groot, *J Synchrotron Radiat*, 2016, **23**, 1264-1271. http://dx.doi.org/10.1107/S1600577516012443.
8. F. M. F. de Groot, J. C. Fuggle, B. T. Thole and G. A. Sawatzky, *Phys Rev B*, 1990, **41**, 928-937. http://dx.doi.org/10.1103/PhysRevB.41.928.